J Nanopart Res (2013) 15:1524
DOI 10.1007/s11051-013-1524-6

RESEARCH PAPER

Finite size effects on the magnetocrystalline anisotropy energy in Fe magnetic nanowires from first principles

F. Muñoz · A. H. Romero · J. Mejía-López · J. L. Morán-López

Received: 8 November 2012 / Accepted: 16 February 2013 / Published online: 27 March 2013

Abstract The geometric and the electronic structures, the magnetic moments, and the magnetocrystalline anisotropy energy of bcc-Fe nanowires with z-axis along the (110) direction are calculated in the framework of ab initio theories. In particular, we report a systematic study of free standing nanowires with geometries and sizes ranging from diatomic to 1 nm wide with 31 atoms per unit cell. We found that for nanowires with less than 14 atoms per unit cell, the ground-state structure is body-centered tetragonal. We also calculated the contributions of the dipolar magnetic energy to the magnetic anisotropy energy and found that in some cases, this contribution overcomes the magnetocrystalline part, determining thereby the easy axis direction. These results emphasize the importance and competition between both contributions in low dimensional systems.

Keywords Magnetic nanowires · Magnetic anisotropy · Magnetic phase transition · Ab initio calculations

Introduction

The development of new experimental techniques to synthesize well-controlled nanostructured materials has attracted renewed interest in low dimensional and confined systems, in the last few decades. The unique physical properties of these systems, due to quantum confinement, are quite interesting, and sometimes

F. Muñoz · A. H. Romero
Max-Planck-Institute für Mikrostrukturphysik, Weinberg 2, 06120 Halle, Germany

F. Muñoz
Departamento de Física, Facultad de Ciencias, Universidad de Chile, Casilla 653, Santiago, Chile

F. Muñoz · J. Mejía-López
Centro para el Desarrollo de la Nanociencia y la Nanotecnología CEDENNA, Avda. Ecuador 3493, Santiago, Chile

A. H. Romero
CINVESTAV, Unidad Querétaro, Libramiento Norponiente 2000, Real de Juriquilla, 76230, Querétaro, Mexico

J. Mejía-López (✉)
Facultad de Física, Pontificia Universidad Católica de Chile, Casilla 306, Av. Vicuña-Mackenna 4860, Santiago 22, Chile
e-mail: jmejia@puc.cl

J. L. Morán-López
Laboratorio Interdisciplinario, Departamento de Física, Facultad de Ciencias, Universidad Nacional Autónoma de México, Mexico, DF, Mexico

unexpected. In particular, special attention has been devoted to the magnetic properties of nanostructures. Due to the enhanced magnetic moment produced by the dimensionality reduction, a natural expectation is to use those materials to produce better and smaller magnetic devices.

It is well known that a key parameter for most applications of magnetic materials is the magnetic anisotropy, which, in turn, is responsible for the hysteresis behavior. The energy needed to magnetize a crystalline sample depends on the direction of the applied magnetic field. The direction in which it takes less energy is known as the easy axis, and it depends on the material and the crystalline structure. Therefore, it is essential to know the magnitude of the local magnetic moments, as well as the energy associated to the magnetic anisotropy, i.e., the magnetic anisotropy energy (MAE), of a given geometric arrangement of atoms. Under bulk conditions, the MAE is fairly small due to the high symmetry of the crystal. On the other hand, in nanostructured materials, the MAE is several orders of magnitude larger (Mokrousov et al. 2006), leading to the possibility of potential technological applications.

In one or quasi-one-dimensional systems, the aspect ratios (length vs width) and the geometric arrangements are of particular relevance. This factor is also known as the shape anisotropy. Thus, a fundamental problem in magnetic 1D (or quasi 1D) materials is the calculation of the MAE to determine how difficult (or easy) it is to magnetize the samples along particular directions.

In general, the MAE has two main sources: the dipolar interaction between atomic magnetic moments, also called the shape anisotropy energy (SAE), and the spin–orbit interaction which gives rise to the so-called magnetocrystalline anisotropy energy (MCAE). The latter contribution arises from the coupling between the spin and the crystal field (i.e., the coupling of the electron spin with the electronic structure produced by the crystal geometry).

Most of the theoretical studies of the MAE in 1D magnetic systems have analyzed only the MCAE contribution. The first calculations performed within the tight-binding model were reported for free Co and Fe chains and a Co chain deposited on a Pd surface (Dorantes-Dávila and Pastor 1998). They calculated the MCAE as a function of the chain length and found that for Fe, the easy axis is along the wire except for the trimer. Later, ab initio density functional calculations of the MCAE were reported for free chains of Fe and Fe wires encapsulated in gold nanotubes (Mokrousov et al. 2005). They report that the easy axis of pure Fe (along the chain axis) is changed when it is covered by gold. Even more, in Fe nanowires (NWs) embedded into carbon nanotubes, a change of the easy axis is also predicted, depending on the specific matching between the NW and the carbon nanotube (Muñoz et al. 2010). Reports on other !D systems include pure Co chains (Hong and Wu 2003) and Co chains deposited in Pt (Shick et al. 2004; Újfalussy et al. 2004). More recent calculations of the 3d, 4d, and 5d transition metal monowires were reported, and it was found that the easy axis direction and the MCAE magnitude changes drastically from one chemical element to the next one (Mokrousov et al. 2006; Tung and Guo 2007, 2010), making it difficult to draw general conclusions.

It is also interesting to note that it has been shown (Tung and Guo 2007, 2010) that the dipole contribution (SAE) to the MAE, which is determined by the geometric shape (SAE), is in some 1D and zig-zag nanowires, as large as the electronic contribution and cannot be neglected. In some cases, the SAE changes the direction of the easy axis.

On the experimental side, recent advances in atomic engineering made it possible to synthesize 1D arrays of transition metal chains on particular substrates. It has been possible to grow Fe arrays on W(110) and Cu(111) surfaces (Hauschild et al. 1998; Shen et al. 1997) and measure their magnetic properties. In the former case, the easy direction of the stripes lies in the surface plane in contrast to the latter one in which the easy axis points in the perpendicular direction. More recently, Co NWs were grown on a vicinal Pt surface (Gambardella et al. 2002). They found a very large magnetic anisotropy, as compared to thin films and bulk Co. Furthermore, the easy axis changes its direction as a function of the transversal shape of the NW, and also as one goes from 1D to quasi 2D atomic arrangements. Other technique to grow magnetic nanowire arrays is to fill nanoporous templates with a well-defined pore geometry (Thurn-Albrecht et al. 2000) with magnetic materials. This method makes use of the self-assembly morphology of asymmetric diblock copolymers, and one can tailor the distance between nanowires to enhance or reduce the inter-wire interactions. Thus, to understand the

behavior of the MAE when changing the transversal section or size, one has to explore the MAE in NWs thicker than a monoatomic chain.

Unfortunately, just a few theoretical studies have addressed the structural and magnetic properties of both, free standing and supported (or embedded) NWs, as a function of its size or transversal shape beyond the biatomic NW. Zelený et al. (2009) calculated within the spin-density functional theory, Fe NWs with unit cells made up to four atoms. They report a structural transition from nanoribbons to nanorods, but the MCAE was not calculated. Furthermore, Dorantes-Dávila and Pastor (2005) performed a systematic study of the MCAE of Fe stripes as a function of stripe width by using a self-consistent tight-binding method. They followed the change of properties from 1D monoatomic chains to 2D films, assuming square and triangular lattices. In the case of thin stripes, an oscillatory behavior of the easy axis is obtained. However, since they found that the dipole contribution is small as compared with the electronic part, they did not take this contribution into account in their final analysis.

The present study aims to cover this gap in free standing Fe NWs, by calculating the structure and the MAEs (magnetocrystalline and dipolar) in NWs with different geometries and sizes, ranging from diatomic unit cells up to NWs, where the number of core atoms is close to the number of surface atoms (unit cells containing 31 atoms).

The layout of the article is as follows. In "Method and computational details" section, our computational approach is presented. Then, in "Structural properties" section, (i) the model used to build the NWs is discussed, as well as (ii) the geometric properties of the optimized NWs. The results for the binding energy and the magnetic moments are presented in "Binding energy and magnetic moments" section. In "Magnetic anisotropy energy" section, the MAEs of the different sized NWs are discussed. Finally, our conclusions are given in "Conclusions" section.

Method and computational details

The calculations were performed using the density functional theory as implemented within the Vienna ab initio simulation package code (Kresse and Hafner 1993, 1994; Kresse and Furthmüller 1996a, b), where the electron wave functions are expanded in a plane wave basis by using the Blöch theorem. Projected–augmented-wave (PAW) type of pseudopotentials were used (Blöchl 1994; Kresse and Joubert 1999) with Perdew–Burke–Erhenzof (PBE) as the exchange–correlation parametrization (Perdew et al. 1996). By using the plane wave expansion and the periodic boundary conditions, we are able to simulate an infinite wire. Therefore, to mimic a single NW and avoid interactions between neighboring cells, perpendicular to the NW axis, a large vacuum slab (at least 10 Å plus the wire width) was considered. We also performed some tests for larger values, of the vacuum slab, to ensure the reliability of our results. Furthermore, the energy cutoff of the plane waves was set at 320 eV. It is important to notice that by reducing the distance between NWs, one can also study the magnetic properties of nanowire arrays.

For all the structures considered here, we first perform a careful ionic relaxation until the forces were negligible, $|\mathbf{F}| < 0.01\ eV/\text{Å}$. We tested that a higher precision on the force limit does not produce any noticeable improvement on the total energies. During the ionic optimization, the cell parameter along the cylinder axis was relaxed; this point is quite important in the case of the thinnest NWs.

With respect to the magnetic configuration, we only considered the ferromagnetic case which corresponds to the ground-state for a free standing Fe NW (Kang et al. 2005; Weissmann et al. 2006). After the total energy minimization, the wave function and charge density were minimized within the collinearity assumption and without spin–orbit coupling. These quantities were used as input for the next step, which corresponds to a noncollinear orientation but without the self-consistent loop. In this last step, the spins are oriented toward the desired crystal direction and the spin–orbit coupling correction is included (Hobbs et al. 2000).

The total energies were calculated by using the afore mentioned procedure, with a convergence criterion of $10^{-7}eV$, in both self-consistent and nonself-consistent loops. We used 30 K-points for all considered nanowires. To test the reliability of this approach, we have performed fully self-consistent calculations, for some specific cases, where the spin–orbit coupling was included from the starting geometric optimization. The MCAE obtained in both cases is almost the same (within the numerical precision). Therefore, we

decided to proceed with the less exhaustive method to avoid highly time consuming calculations.

Structural properties

Model structure

The initial structures, before the geometric relaxation, are built from a cylindrical cut along the (110) direction of the bcc phase of bulk iron. The length of the periodicity along the cylinder axis (ρ), in the nonrelaxed NWs, is 4.06 Å (see Fig. 1). It is interesting to note that this periodicity is close to the zigzag carbon nanotubes, and therefore offers interesting possibilities in the study of encapsulated NWs in these nanotubes (Muñoz et al. 2010; Weissmann et al. 2006).

To see the role of the underlying symmetry, we also modeled NWs with a hexagonal (0001) symmetry (the hcp axis is along the NW axis). In this case, the assumed nearest neighbors distance is the same as in bcc iron. Although bulk ferromagnetic iron is bcc, the hcp lattice is a good candidate to make NWs, due to their high coordination-like the (111) fcc- and that the unit cell has two layers by unit cell, similar to (110) bcc.

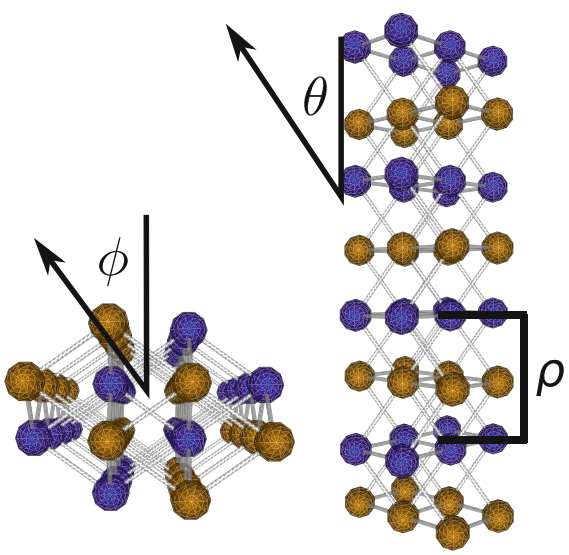

Fig. 1 Transversal and longitudinal views of a nanowire before the structural optimization (bcc in this case, but the hcp NWs is quite similar). The unit cell size along the periodic axis is denoted by ρ. Each unit cell consists of two layers: one with *blue* (dark) and the other with *orange* (clear) atoms. The angle between the z-axis and the magnetization is denoted by θ, and ϕ is the azimuthal angle in the plane xy. (Color figure online)

We considered all the possible cylindrical nonrelaxed arrangements with diameter less than 1 nm; i.e., depending on the diameter, the axis of the cylinder may pass though Fe atoms, through the middle of a Fe-Fe bond, etc. This procedure generates a set of NWs, not only with different diameters, but also by obeying different symmetry operations (like reflection and inversion).

The original structures of both bcc and hcp NWs have a unit cell composed of two layers. In general, the atoms in both layers have the same geometric arrangements but their orientations may differ. However, some NWs do not follow this trend, and have a different number of atoms in each layer. In this report, the unit cell size ranges from $N = 2$–31 atoms.

Ground-state geometric structures

In general, the calculations of NWs, thicker than one (mono-atomic chain) or two (biatomic zigzag arrangements) atoms per unit cell, reported by other authors, were performed neglecting the structural optimization along the periodicity axis (Weissmann et al. 2006). However, because a large number of surface atoms are under-coordinated, a significant stress is generated. Thus, it is important to allow relaxation in all the cases. We observed that the optimization of the atomic coordination in the unit cell, modifies the cell parameter along the nanotube axis ρ, producing thereby a higher coordination and/or stronger bonding.

In the bcc NWs, the cell height ρ shows an abrupt transition when the number of atoms per unit cell reaches the value of 14 (see circles in Fig. 2). In NWs with unit cells made of a smaller number of atoms, ρ takes a value close to 2.7 Å, and their geometry changes to a body-centered tetragonal along the (001) direction. The relaxed lattice parameter is $a \approx 4$Å, i.e., the cells are wider and thinner after relaxation. The shortest value for ρ corresponds to the NW with three atoms per unit cell. The compression is driven by the increase of the interaction between biatomic layers (the other layers have only one atom lying between the two atoms in neighboring layers). The NWs with 14 or more atoms per unit cell, preserve almost their bcc shape; the relaxation produces only minor changes.

Therefore, the observed transition is attributed to the low coordination number of systems with less than

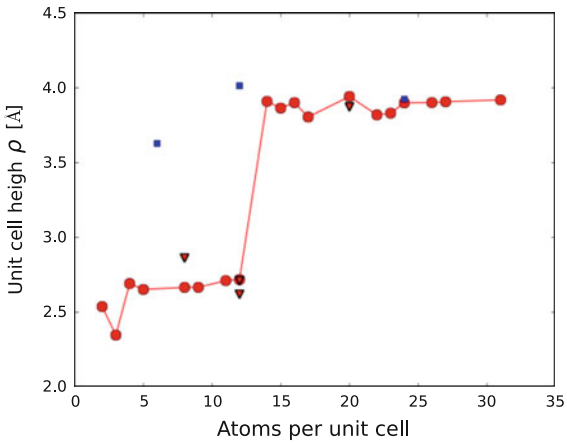

Fig. 2 Optimized unit cell height ρ (in Å) along the NW axis. The ground-state values are marked by *circles* and joined by a *line*. The structures assumed with a hcp symmetry, before relaxation, are marked by *squares*. The isomeric structures for some NWs, with smaller binding energy, are marked by *triangles*

14 atoms, which reduces the unit cell height to increase the interaction between atoms. This reduction of the unit cell in the axis direction changes the symmetry from body-centered-cubic to body-centered tetragonal.

Assuming a hcp starting structure (with two predefined lattice parameters a and ρ), the only NWs that maintain this structure are those with 6, 12, and 24 atoms per unit cell (denoted by squares). The one with $N = 6$ is the only one more stable than the bcc arrangement, although it has a ρ value much larger than the NWs with similar number of atoms. For $N = 12$, the hcp structure has a much larger ρ than those of the bcc geometries. Finally, the hcp structure with $N = 24$ has a very similar ρ to the bcc but it has a weaker binding energy. In the case of the hexagonal, there are different possibilities as to how the nanotube can be obtained from the crystalline structure; this allowed us to construct different potential structures which all were relaxed. The isomers with lower binding energy are denoted by inverted triangles in Fig. 2.

We show in Fig. 3 the cross sections of all the relaxed NWs. As mentioned above, the blue (dark) and orange (clear) atoms are located in neighboring layers. The arrows below the structures give information of the magnetic easy axis, discussed in the next section. This figure shows all the geometric arrangements considered in this article. In the case of various arrangements for the same N, the ones labeled (a) are those with the strongest binding energy.

Due to these structural transitions, the NW diameter is not appropriate to classify the NWs; instead, we will use the number of atoms per unit cell, although from an experimental point of view, the meaningful parameter to characterize the NWs is their diameter. In Table 1, we give in the second column, the ground-state geometry for each nanowire. Then, in columns 3 and 4, the major and minor diameters (fitting an ellipse) of the relaxed NWs are reported. The last column contains the nearest neighbor distance d_{NN} in Å. We refer to the wires as bcc-like or hcp-like, only when an NW after the relaxation resembles this symmetry. Although, due to the surface effects, this classification is not exact, e.g., a simple inspection makes evident that the six-fold rotational symmetry in the hcp-like 6 and 12*d* NWs is not preserved. Although this feature is present, it is less evident in the case 24*b*. The nearest neighbors distance (d_{NN}) is a complex function of the NW size because it is greatly affected by the cross-sectional shape. When the shape is cylindrical (4, 9, 12, 24b, and 31), d_{NN} is a maximum. Instead, when the cross section is elongated (8*b*, 12*c*) or the NW has sharp edges (8, 11, 22, and 27), d_{NN} is a minimum.

Binding energy and magnetic moments

In the upper panel of Fig. 4, we show the average magnetic moment per atom in Bohr magnetons

$$\bar{\mu} = \frac{1}{N}\sum_i \mu_i, \tag{1}$$

as a function of the number of atoms per unit cell N. The results for the ground-state structures are represented by circles. In the case of structures with isomers, b, c, or d, (see Fig. 3) the results are shown by stars, down, and side-triangles, respectively.

The average magnetic moment shows, in general, a smooth decrease as a function of N. However, due to the complex surface atomic structure (the less coordinated atoms have a greater magnetic moment), some small oscillations are present. In all cases, the average magnetic moment is larger than in the bulk, which is expected since in all the cases more than half of the atoms are at the surface. The only point that does not

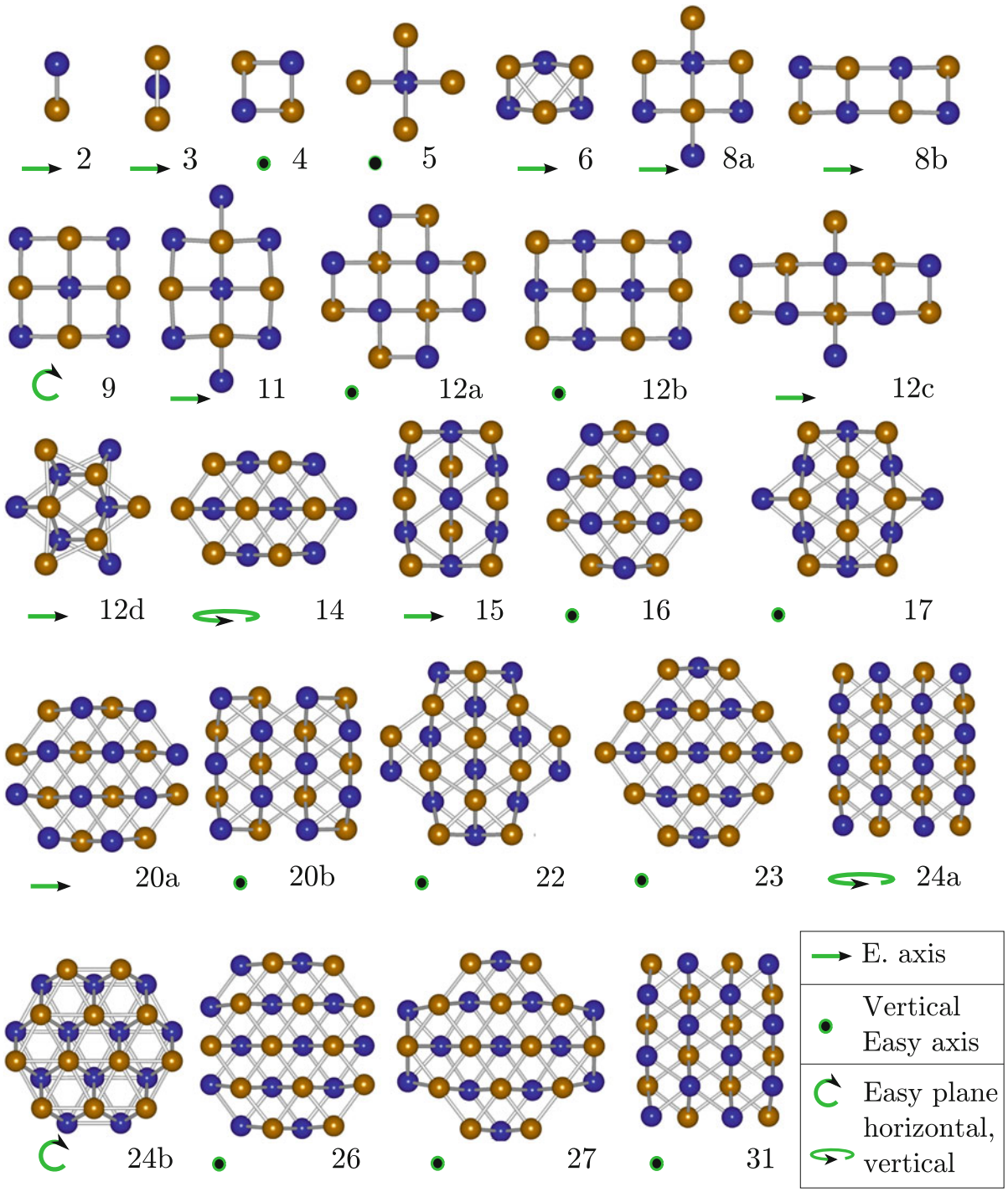

Fig. 3 Views of the relaxed unit cells perpendicular to the periodicity axis. Each *color* represents a different layer: the *upper layer* is *orange* (clear) and the *lower* is *blue* (dark). The number below each NW is the number of atoms in the unit cell. NWs with the same number of atoms are labeled by their stability (the ground-state is labeled 'a', and so on). The magnetic easy axis of each NW is denoted by the *arrows* or *dots* bellow the structures. (Color figure online)

Table 1 Number of atoms per unit cell N (the isomers are labeled according to Fig. 3), crystal structure, major diameter D_a, minor diameter D_b, and the nearest neighbors distance (d_{NN}) of the NWs

N	Structure	D_a	D_b	d_{NN}
2	zig-zag	1.83	0.00	2.22
3	ribbon	4.22	0.00	2.34
4	tetr	2.75	2.75	2.37
5	tetr	3.84	3.84	2.33
6	hcp	4.10	2.51	2.36
8	tetr	5.86	4.39	2.28
8b	tetr	8.35	2.86	2.26
9	tetr	5.73	5.73	2.43
11	tetr	7.92	4.80	2.32
12a	tetr	6.32	6.32	2.39
12b	tetr	8.55	6.00	2.38
12c	tetr	8.56	5.72	2.36
12d	hcp	6.23	5.42	2.34
14	bcc	6.90	4.77	2.34
15	bcc	7.79	5.81	2.38
16	bcc	6.38	6.12	2.36
17	bcc	7.50	6.94	2.31
20a	bcc	7.48	6.60	2.34
20b	bcc	8.07	7.78	2.32
22	bcc	8.08	8.00	2.30
23	bcc	8.71	8.14	2.34
24a	bcc	9.70	8.07	2.31
24b	hcp	7.64	7.47	2.39
26	bcc	8.92	8.03	2.36
27	bcc	9.19	8.30	2.29
31	bcc	9.65	9.56	2.42

follow this trend, with a value close to bulk (2.2 μ_B), corresponds to the NW labeled as 24*b*. This small value is produced by the hcp-like symmetry; the atoms at the inner triangles possess a magnetic moment $\approx 1.5\ \mu_B$.

To illustrate how the atomic magnetic moments depend on their local geometric environment, in Fig. 5, we give the values of the magnetic moments that correspond to the atoms with different environments of the NW with $N = 17$. The highest and the lowest values, $\mu = 3\ \mu_B$, $2.4\ \mu_B$, correspond to the less-coordinated atom and the one in the center, respectively. All other atoms have magnetic moments with values in between those values.

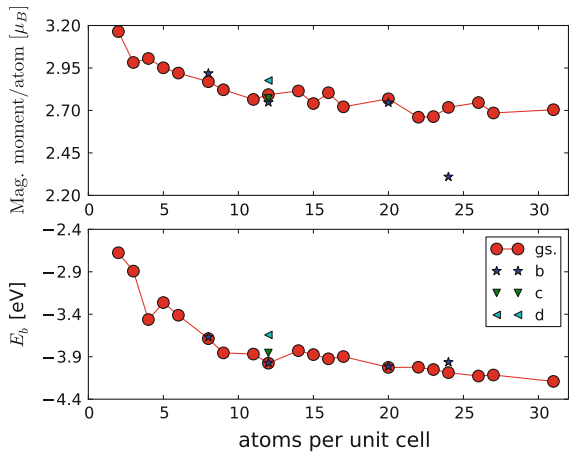

Fig. 4 Average magnetic moment per atom $\bar{\mu}$ (*upper panel*) in Bohr magnetons, and binding energy E_b (*lower panel*) in electron Volts, of the relaxed NWs as a function of the number of atoms per unit cell N. The line joining ground-state structures (*circles*) is just a guide to the eye. The isomers are labeled according to Fig. 3

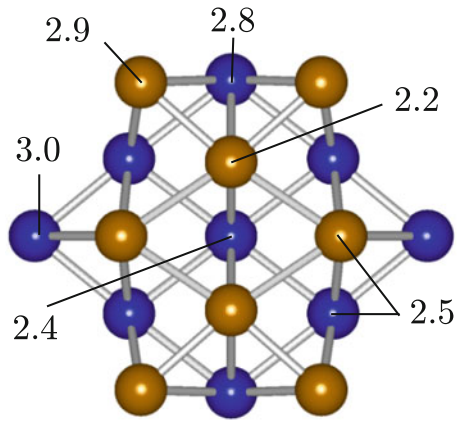

Fig. 5 Values of the magnetic moments, μ_i in Bohr magnetons, of the atoms with different geometric environments corresponding to the nanowire with $N = 17$. Each *color* represents a different layer: the *upper layer* is *orange* (clear) and the *lower* is *blue* (dark). (Color figure online)

In the lower panel, we show the N-dependence of the binding energy E_b. It decreases as a function of N toward the bulk value, but it is important to note that there are local minima ('magic sizes') corresponding to wires with 4 and 12 atoms per unit cell. These NWs are more compact (i.e., they have a nearly cylindrical shape), as compared to the structures with smaller and larger N.

Magnetic anisotropy energy

As mentioned above, the MAE has two main sources: the shape anisotropy energy (SAE) and the MCAE. We calculated these two contributions in all the NWs described in the previous section.

Magnetocrystalline anisotropy energy

To study the magnetocrystalline anisotropies, we align the magnetic moments along a desired direction and calculate the total energy (including the spin–orbit coupling). To a good approximation, due to the cylindrical symmetry, the total energy as a function of the magnetization orientation (θ, ϕ), with respect to the NW axis, can be written as (Tung and Guo 2007)

$$E(\theta,\phi) = E_0 + \sin^2(\theta)\big(K_1 + K_2\cos^2(\phi)\big), \qquad (2)$$

where θ is the angle that forms the magnetization with the z-axis (NW axis), and ϕ is the azimuthal angle in the plane xy. The anisotropy constant $K_1 = E(\pi/2, \pi/2) - E(0, 0)$ is the axial contribution; a positive value means that the easy axis is along the NW axis, and a negative one is obtained when the easy axis is in the perpendicular plane. K_2 is the difference between the maximum and minimum values of $E(\pi/2, \phi)$ as one sweeps the magnetization on the xy plane. When the NW has fourfold symmetry (or twofold plus inversion), K_2 becomes negligible and the anisotropy in-plane disappears.

Operationally, we first calculated the MCAE in the plane xy by rotating the magnetization in intervals of 10°, and identified the maxima and minima. We defined $\phi = 0$ at the position of maximum energy. Then, we calculated the axial MCAE by rotating the magnetization through angles of the same magnitude, from $\theta = 0$ to $\pi/2$, and keeping $\phi = \pi/2$ (minimum in plane energy). With these definitions, K_2 is always positive.

The energy as a function of the magnetic orientation θ and ϕ for the NW with $N = 3$ is presented in Fig. 6. The left side corresponds to the rotation of the magnetization from the z axis ($\theta = 0$) to the y axis ($\theta = \pi/2$, $\phi = \pi/2$). The right side shows how the energy changes as we rotate the magnetization, from this orientation, on the plane xy to $\phi = \pi$. The zero of energy is taken at E_0 (axial magnetization). In this case, the easy axis is perpendicular to the z and along y.

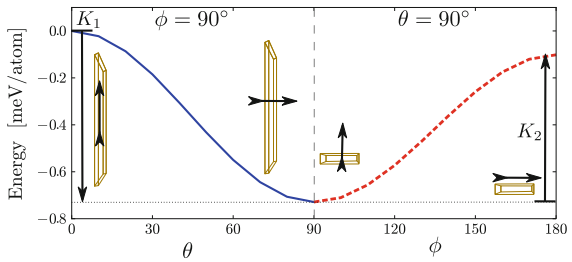

Fig. 6 *Left side* the energy as a function of the magnetic orientation θ keeping $\phi = \pi/2$. *Right side* the energy as a function of the magnetization orientation ϕ, in the plane xy

In Fig. 7, we present the dependence of K_1 (upper panel) and K_2 (lower panel) as a function of the number of atoms in the unit cell. We found that based on the MCAE, the easy axis always lies perpendicular to the axial orientation. It is interesting that the ribbon-like NWs (with two and three atoms per unit cell) have the largest MCAE. A similar result for the zig-zag NW ($N = 2$) was obtained before (Tung and Guo 2007, Dorantes-Dávila and Pastor 2005). Tung and Guo obtained a value of −0.7 and 0.58 meV/atom, and Dorantes-Davila and Pastor about −2 and 2 meV/atom, for K_1 and K_2, respectively. In our case, we obtain $K_1 = -0.51$ and $K_2 = 0.46$. In Table 2, we compare our results to those obtained previously.

In thicker NWs, their shape loses the 2D characteristics, and the magnetic anisotropy constants, K_1

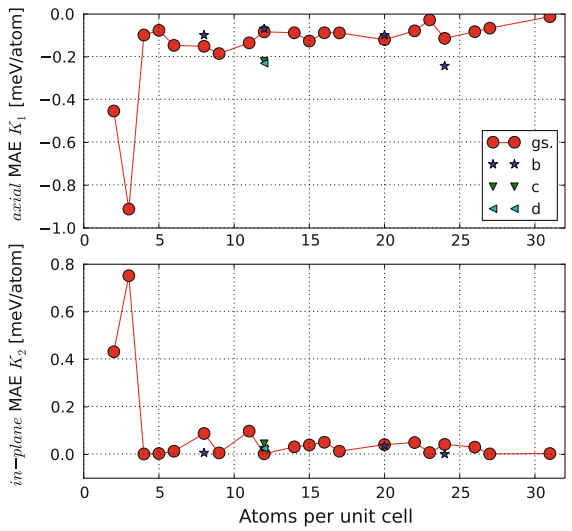

Fig. 7 Axial (K_1) and in-plane (K_2) components of the MCAE, according to Eq. 2. The line joining ground-state structures is just a guide to the eye. The isomers are labeled according to Fig. 3. A negative K_1 means an *in-plane* easy axis

Table 2 Comparison of the MAE parameters K_1 and K_2, as obtained in our study with the values reported in Ref. (Tung and Guo 2007; Dorantes-Dávila and Pastor 2005). The total, the MCAE and the dipolar contributions are denoted by the superscripts t, e, and d, respectively, and are given in meV/atom

	K_1^e	K_2^e	K_1^d	K_2^d	K_1^t	K_2^t
This study	−0.51	0.46	0.2	−0.1	−0.31	0.36
Ref. (Tung and Guo 2007)	−0.70	0.58	0.37	0.19	−0.33	0.39
Ref. (Dorantes-Dávila and Pastor 2005)	−2.0	2.0			−2.0	2.0

and K_2, rapidly decrease. NWs with high in-plane symmetry, like $N = 4$, 5, and 12a, do not posses any appreciable in-plane component of the anisotropy (i.e., they have an easy plane). We observe that the hcp-like NWs have a larger MCAE than that of bcc NWs. This behavior is because the hcp lattice axis coincides with the NW axial axis. The thicker bcc-like NWs have a smaller anisotropy per atom than the thin ones, but in average, their MCAE is $\approx$50 times larger than in bulk iron.

Dipolar energy

The dipolar interaction energy, also known as the shape anisotropy energy (SAE), of a set of magnetic moments μ_i, located in a given geometric arrangement, is given by

$$E_i = -\frac{\mu_0}{4\pi}\sum_j \frac{1}{r_{ij}^3}[3(\mu_i \cdot \mathbf{e}_{ij})(\mu_j \cdot \mathbf{e}_{ij}) - \mu_i \cdot \mu_j], \qquad (3)$$

where μ_0 is the vacuum permeability, r_{ij} is the distance between μ_i and μ_j and its vector is directed along the direction $\mathbf{e}_{ij}$. The sum has to be calculated taking into account an infinite number of magnetic moments (our nanowires are considered infinite). In practice, we sum up to a number of cells until the difference between two successive steps is less than a given tolerance (of the order of 1,000 steps). We obtained an analytic expression only when the magnetic moments of a monoatomic linear chain are oriented along the z-axis. In this case, the energy is given by

$$E_i = -\frac{\mu_0 \mu^2 \zeta(3)}{2\pi L^3}, \qquad (4)$$

where μ is the atomic magnetic moment, $\zeta(3) \approx 1.2$ is the Riemann function, and L is the nearest neighbor distance.

We calculated the SAE by a procedure similar to the MCAE and obtained the corresponding K_1^d and K_2^d values.

The results for the anisotropy constants K_1 and K_2 for the studied NWs are given in Table 3. Here, we give the total values (t) and their components; magnetocrystalline (e) and dipolar (d). In contrast to the K_1^e , the K_1^d is always positive. As expected, this contribution drives in favor of an axial easy axis. However, only in some cases, $|K_1^d| > |K_1^e|$, i.e., $N = 4$, 5, 12a, 12b, 16, 17, 20b, 22, 26, 27, and 31. As mentioned above, it is important to note that NWs with high in-plane symmetry do not possess an in-plane component of the anisotropy, giving rise to an easy plane. From Table 3, one observes that K_2^d is zero (within our tolerance) for the structures with $N = 4$, 5, 9, 12a, 17, 20b, 22, 23, 24b, and 31.

In Fig. 3, we show below the various structures the direction of easy axis: when it lies on the plane perpendicular to the z-axis, it is denoted by an arrow; when it coincides with the z-axis, it is represented by a dot. Easy plane perpendicular to or along the z-axis is denoted by a circle or and an ellipse, respectively. This figure shows the large variety of magnetic behaviors that depend on the geometric structure and the number of atoms in the cell.

Conclusions

A complete structural optimization of Fe NWs, with less than 32 atoms per unit cell i.e., 1 nm wide, was performed. The NWs were built from bcc iron with axis along (110) direction, and for comparison, we considered also hcp NWs, in some cases. A strong dependence of the cell height ρ on the number of atoms by unit cell was observed. For structures with unit cells with less than 12 atoms, the cross section suffers a transition to a tetragonal-body-centered structure. For NWs with larger unit cells, it preserves the bcc structure with the original cell height, but with a relaxed surface. From this effect, we concluded that

Table 3 The anisotropy constants K_1 and K_2 for the various nanowires. The total, the MCAE, and the dipolar contributions are denoted by the superscripts *t*, *e*, and *d*, respectively, and are given in meV/atom

	Total		MCAE		Dipolar	
	K_1^t	K_2^t	K_1^e	K_2^e	K_1^d	K_2^d
2	−0.31	0.36	−0.51	0.46	0.2	−0.1
3	−0.72	0.63	−0.91	0.75	0.19	−0.12
4	0.02	0	−0.1	0	0.12	0
5	0.03	0	−0.08	0	0.11	0
6	−0.04	0.04	−0.14	0.01	0.1	0.03
8a	−0.04	0.07	−0.16	0.09	0.12	−0.02
8b	−0.03	0.06	−0.1	0	0.07	0.06
9	−0.08	0	−0.19	0	0.11	0
11	−0.02	0.06	−0.14	0.1	0.12	−0.04
12a	0.02	0	−0.09	0	0.11	0
12b	0.02	0.06	−0.07	0.03	0.09	0.03
12c	−0.13	0.08	−0.22	0.04	0.09	0.04
12d	−0.12	0.01	−0.23	0.02	0.11	−0.01
14	0	0.06	−0.09	0.03	0.09	0.03
15	−0.02	0.02	−0.14	0.04	0.12	−0.02
16	0.01	0.04	−0.09	0.05	0.1	−0.01
17	0.01	0.01	−0.08	0.01	0.09	0
20a	−0.03	0.05	−0.12	0.04	0.09	0.01
20b	0.01	0.03	−0.1	0.03	0.11	0
22	0.01	0.05	−0.08	0.05	0.09	0
23	0.06	0	−0.03	0	0.09	0
24a	0	0.02	−0.11	0.04	0.11	−0.02
24b	−0.16	0	−0.24	0	0.08	0
26	0.02	0.02	−0.08	0.03	0.1	−0.01
27	0.03	0.01	−0.07	0	0.1	0.01
31	0.08	0	−0.02	0	0.1	0

one must always relax the structure along the axial direction.

The average magnetic moment of all NWs is larger than the one in the bulk and decreases slowly as a function of the number of atoms per unit cell. However, due to the different surface atomic structures (the less-coordinated atoms have a greater magnetic moment), some small oscillations are observed.

The binding energy E_b decreases as a function of N toward the bulk value, but there are local minima that correspond to wires with a nearly cylindrical shape (four and 12 atoms per unit cell).

We calculated the magnetocrystalline and dipolar contributions to the MAE. The axial contributions ($K_1^{e(p)}$) are opposite in sign and of very similar magnitude. This gives rise to changes of the easy axis direction, from the z-axis to the perpendicular plane. Furthermore, in very symmetric structures, we even obtained an easy plane.

To our knowledge, this is the first systematic study of the interplay between the dipolar and crystalline contributions to the anisotropy magnetic energy in nanowires, as a function of its diameter.

Acknowledgements The authors gratefully acknowledge the support from FONDECYT 1100365 (J.M.-L.) and 11110510 (F.M.), Grant ICM P10-061-F by "Fondo de Innovación para la competitividad-MINCOM (J.M.-L and F.M.), Financiamiento Basal para Centros Científicos y Tecnológicos de Excelencia, under project FB0807 (J.M.-L.) and CONACYT (Mexico) through grants 61417 (J.L.M.), J-59853-F (J.L.M.), and J-152153-F (A.H.R). A.H.R. also acknowledges the support from the binational program TAMU-CONACYT and the Marie-Curie Intra-European Fellowship and the support of CONACYT-Mexico for the sabbatical program. The use of computational resources from the CNS, IPICyT is acknowledged.

References

Blöchl P (1994) Projector augmented-wave method. Phys Rev B 50(24):17953–17979

Dorantes-Dávila J, Pastor GM (1998) Magnetic anisotropy of one-dimensional nanostructures of transition metals. Phys Rev Lett 81:208–211

Dorantes-Dávila J, Pastor GM (2005) Magnetic reorientation transitions along the crossover from one-dimensional to two-dimensional transition-metal nanostructures. Phys Rev B 72:085427

Gambardella P, Dallmeyer A, Maiti K, Malagoli M, Eberhardt W, Kern K, Carbone C et al (2002) Ferromagnetism in one-dimensional monatomic metal chains. Nature 416(6878):301–304

Hauschild J, Elmers HJ, Gradmann U (1998) Dipolar superferromagnetism in monolayer nanostripes of fe(110) on vicinal w(110) surfaces. Phys Rev B 57:R677–R680

Hobbs D, Kresse G, Hafner J (2000) Fully unconstrained non-collinear magnetism within the projector augmented-wave method. Phys Rev B 62(17):11556–11570

Hong J, Wu RQ (2003) First principles calculations of magnetic anisotropy energy of co monatomic wires. Phys Rev B 67:020406

Kang YJ, Choi J, Moon CY, Chang KJ (2005) Electronic and magnetic properties of single-wall carbon nanotubes filled with iron atoms. Phys Rev B 71:115441

Kresse G, Furthmüller J (1996a) Efficiency of ab-initio total energy calculations for metals and semiconductors using a plane-wave basis set. J Comput Mater Sci 6:15–50

Kresse G, Furthmüller J (1996b) Efficient iterative schemes for ab initio total-energy calculations using a plane-wave basis set. Phys Rev B 54(16):11169–11186

Kresse G, Hafner J (1993) *Ab initio* molecular dynamics for liquid metals. Phys Rev B 47(1):558–561

Kresse G, Hafner J (1994) Ab initio molecular-dynamics simulation of the liquid-metal amorphous-semiconductor transition in germanium. Phys Rev B 49(20):14251–14269

Kresse G, Joubert D (1999) From ultrasoft pseudopotentials to the projector augmented-wave method. Phys Rev B 59(3):1758–1775

Mokrousov Y, Bihlmayer G, Blügel S (2005) Full-potential linearized augmented plane-wave method for one-dimensional systems: Gold nanowire and iron monowires in a gold tube. Phys Rev B 72:045402

Mokrousov Y, Bihlmayer G, Heinze S, Blügel S (2006) Giant magnetocrystalline anisotropies of 4*d* transition-metal monowires. Phys Rev Lett 96:147201

Muñoz F, Mejía-López J, Pérez-Acle T, Romero A (2010) Uniaxial magnetic anisotropy energy of fe wires embedded in carbon nanotubes. ACS Nano 4(5):2883–2891

Perdew J, Burke K, Ernzerhof M (1996) Generalized gradient approximation made simple. Phys Rev Lett 77(18): 3865–3868

Shen J, Skomski R, Klaua M, Jenniches H, Manoharan SS, Kirschner J (1997) Magnetism in one dimension: Fe on cu(111). Phys Rev B 56:2340–2343

Shick A, Máca F, Oppeneer P (2004) Anomalous ferromagnetism of a monatomic co wire at the pt(111) surface step edge. Phys Rev B 69:212410

Thurn-Albrecht T, Schotter J, Kästle G, Emley N, Shibauchi T, Krusin-Elbaum L, Guarini K, Black C, Tuominen M, Russell T (2000) Ultrahigh-density nanowire arrays grown in self-assembled diblock copolymer templates. Science 290(5499):2126–2129

Tung JC, Guo GY (2007) Systematic ab initio study of the magnetic and electronic properties of all 3*d* transition metal linear and zigzag nanowires. Phys Rev B 76:094413

Tung JC, Guo GY (2010) Magnetic moment and magnetic anisotropy of linear and zigzag 4*d* and 5*d* transition metal nanowires: First-principles calculations. Phys Rev B 81:094422

Újfalussy B, Lazarovits B, Szunyogh L, Stocks GM, Weinberger P (2004) *Ab initio* spin dynamics applied to nanoparticles: Canted magnetism of a finite Co chain along a Pt(111) surface step edge. Phys Rev B 70:100404

Weissmann M, García G, Kiwi M, Ramírez R, Fu C-C (2006) Theoretical study of iron-filled carbon nanotubes. Phys Rev B 73:125435

Zelený M, Šob M, Hafner J (2009) Ab initio density functional calculations of ferromagnetism in low-dimensional nanostructures: From nanowires to nanorods. Phys Rev B 79:134421